Supplementary Information:
Uniformly polarized multi-output illumination by metasurfaces performing near-complete conversion of unpolarized light

Neuton Li,[1,*] Shaun Lung,[1,2] Jihua Zhang,[1,3]
Dragomir N. Neshev,[1] and Andrey A. Sukhorukov[1,†]

[1]*ARC Centre of Excellence for Transformative Meta-Optical Systems (TMOS), Department of Electronic Materials Engineering, Research School of Physics, Australian National University, Canberra, ACT 2600, Australia*

[2]*Abbe Center of Photonics, Friedrich-Schiller Universität, Albert-Einstein-Straße 15, 07745 Jena, Germany*

[3]*Songshan Lake Materials Laboratory, Dongguan, Guangdong 523808, P. R. China*

(Dated: August 21, 2024)

This Supporting Information contains 12 sections and 11 figures, which provide extra details on the theoretical and experimental aspects of our work.

* Neuton.Li@anu.edu.au
† Andrey.Sukhorukov@anu.edu.au

CONTENTS

S1. FUNDAMENTALS OF SPLITTING UNPOLARIZED TO POLARIZED LIGHT

We identify the fundamental properties of linear optical devices, where unpolarized light is coupled to a single input port, while fully polarized light emerges from each of the N output ports. Mathematically, the transformation of input to each output can be defined by a Jones matrix, which we can express using singular value decomposition (SVD) as follows:

$$\mathbf{J}_n = \mathbf{U}_n \begin{pmatrix} A_n & 0 \\ 0 & 0 \end{pmatrix} \mathbf{V}_n^*, \tag{S1}$$

where n is the number of the output port, $\mathbf{U}_n$ and $\mathbf{V}_n$ are unitary matrices. The first singular value is A_n, which is bounded for passive devices as $0 \leq A_1 \leq 1$. The second value is taken as 0, such that each output transformation is similar to a perfect polarizer, only transmitting light with a single polarization.

For the subsequent analysis, it is convenient to introduce parameters θ_n, φ_n, and $\tilde{\varphi}_n$ that define the unitary matrix

$$\mathbf{V}_n^*(\mathbf{V}_1^*)^{-1} = \begin{pmatrix} \cos(\theta_n) & \sin(\theta_n)e^{i\varphi_n} \\ -\sin(\theta_n)e^{-i\varphi_n - 2i\tilde{\varphi}_n} & \cos(\theta_n)e^{-2i\tilde{\varphi}_n} \end{pmatrix}, \tag{S2}$$

where we absorbed the global phase into $\mathbf{V}_n$ with no loss of generality. By construction, $\theta_1 = 0$ and $\varphi_1 = 0$, and we can also set $\varphi_2 = 0$ by absorbing this phase into $\mathbf{V}_1$.

Then, we rewrite Eq. (S1) in an equivalent form,

$$\mathbf{J}_n = \mathbf{J}_n(\mathbf{V}_1^*)^{-1}\mathbf{V}_1^* = \mathbf{U}_n \begin{pmatrix} A_n\cos(\theta_n) & A_n\sin(\theta_n)e^{i\varphi_n} \\ 0 & 0 \end{pmatrix} \mathbf{V}_1^*. \tag{S3}$$

For a passive device, the output power cannot exceed the input. Considering an arbitrary fully polarized input state of unity power in the form

$$|\Psi_{\text{in}}\rangle = (\mathbf{V}_1^*)^{-1} \begin{pmatrix} \cos(\alpha) \\ \sin(\alpha)\exp(i\xi) \end{pmatrix}, \tag{S4}$$

the corresponding output power is

$$P_{\text{pol,total}} = \sum_{n=1}^{N} |A_n|^2 \left|\cos(\alpha)\cos(\theta_n) + \sin(\alpha)\sin(\theta_n)\exp(i\varphi_n + i\xi)\right|^2, \tag{S5}$$

and we demand that $P_{\text{pol,total}} \leq 1$ for all (α, ξ).

An unpolarized input light of unity power can be represented using a density matrix as

$$\rho_{\text{in}} = \frac{1}{2}(|H\rangle\langle H| + |V\rangle\langle V|) = \begin{pmatrix} 1/2 & 0 \\ 0 & 1/2 \end{pmatrix} . \tag{S6}$$

The corresponding power at each of the output ports is then found as

$$P_{\text{unpol},n} = \frac{1}{2}|A_n|^2 , \tag{S7}$$

and the total output power is

$$P_{\text{unpol,total}} = \frac{1}{2}\sum_{n=1}^{N}|A_n|^2 . \tag{S8}$$

We now consider the properties and limitations of devices with different numbers N of output ports.

S1.1. $N = 1$ output port

According to Eq. (S5), $|A_1| \leq 1$. Then, from Eq. (S8) we see that the maximum conversion efficiency from unpolarized to polarized light is 50% (when $|A_1| = 1$), as with a conventional polarizer.

S1.2. $N = 2$ output ports

A device can achieve 100% transmission from an unpolarized input, as well as from any polarized input, such that $P_{\text{unpol,total}} = P_{\text{pol,total}} \equiv 1$, when $|A_1|^2 = |A_2|^2 = 1$, $\theta_1 = 0$, and $\theta_2 = \pi/2$. Note that exactly 50% of unpolarized light is transmitted to each of the two output ports. This is analogous to the operation of a conventional polarization beam splitter, whereas the metasurface can also prepare the outputs to be in the same (rather than orthogonal) polarization state. This also implies that if a polarization states is maximally (up to 100%) transmitted to one output, then its orthogonal state must be maximally transmitted to the other output.

S1.3. $N = 3$ output ports

Similar to the previous case of $N = 2$, a three-port device can also achieve 100% transmission from an unpolarized input, as well as from any polarized input, such that $P_{\text{unpol,total}} = P_{\text{pol,total}} \equiv 1$.

A fundamental distinction from $N = 2$ is that there appears *full flexibility in how the unpolarized light is split between the three output ports*, with the only restriction that each port output cannot exceed 50% according to Eq. (S7) and noting that $|A_n|^2 \leq 1$ while $\sum_n |A_n|^2 = 2$.

Indeed, we find an explicit analytical form of the Jones matrix that allows such flexible splitting with

$$\begin{aligned} &\theta_1 = 0, \quad \varphi_1 = \varphi_2 = \varphi_3 = 0\,, \\ &\theta_2 = \arctan\left(\frac{\sqrt{1-|A_1|^2}\sqrt{1-|A_2|^2}}{\sqrt{1-|A_3|^2}}\right), \\ &\theta_3 = -\arctan\left(\frac{\sqrt{1-|A_1|^2}\sqrt{1-|A_3|^2}}{\sqrt{1-|A_2|^2}}\right). \end{aligned} \tag{S9}$$

S1.4. $N \geq 4$ output ports

For a larger number of output ports, one can also determine a physical Jones matrix for 100% efficiency and arbitrary splitting of unpolarized input between the fully polarized outputs, subject to 50% maximum to an individual output. Indeed, there are $(N-1)+(N-2) = 2N-3$ free parameters ($\theta_{2,\ldots,N}$ and $\varphi_{3,\ldots,N}$). On the other hand, by analyzing Eq. (S5) we find that the requirement of $P_{\text{unpol,total}} = P_{\text{pol,total}} \equiv 1$ is satisfied when the following relations are fulfilled simultaneously:

$$\begin{aligned} &\sum_{n=1}^{N} |A_n|^2 \left|\cos(\theta_n)\right|^2 = 1, \\ &\sum_{n=1}^{N} |A_n|^2 \sin(2\theta_n)\cos(\varphi_n) = 0, \\ &\sum_{n=1}^{N} |A_n|^2 \sin(2\theta_n)\sin(\varphi_n) = 0, \end{aligned} \tag{S10}$$

where we consider $\sum_n |A_n|^2 = 2$ according to Eq. (S8). Since the number of free parameters exceeds the number of conditions in Eq. (S10), i.e. $2N-3 > 3$ for $N \geq 4$, there, in general, appear multiple (non-unique) solutions.

We explicitly determine a particular solution with $\varphi_n \equiv 0$. Let us partition all output port numbers into three subsets $\mathcal{N}_q$, such that $|\tilde{A}_q|^2 = \sum_{n\in\mathcal{N}_q} |A_n|^2 \leq 1$ for $q = 1, 2, 3$. We can prove that such a partition is always possible using recursion, by noting that for $N \geq 4$, the two smallest elements $|A_n|^2$ can be combined in a subset with their sum not exceeding $4/N \leq 1$. Then, a

solution is found as

$$\begin{aligned}
\theta_{n\in\mathcal{N}_1} &= 0\,, \\
\theta_{n\in\mathcal{N}_2} &= \arctan\left(\frac{\sqrt{1-|\tilde{A}_1|^2}\sqrt{1-|\tilde{A}_2|^2}}{\sqrt{1-|\tilde{A}_3|^2}}\right), \\
\theta_{n\in\mathcal{N}_3} &= -\arctan\left(\frac{\sqrt{1-|\tilde{A}_1|^2}\sqrt{1-|\tilde{A}_3|^2}}{\sqrt{1-|\tilde{A}_2|^2}}\right).
\end{aligned} \tag{S11}$$

Note that the above solution reduces to Eq. (S11) for $N = 3$.

We demonstrate a metasurface with $N = 4$ polarized outputs in Sec. S12.

S2. ACHIEVING POLARIZATION CONVERSION AND SPLITTING WITH CONVENTIONAL OPTICAL COMPONENTS

For comparison, we discuss a conversion of unpolarized input to identically purely polarized outputs using conventional optical components.

With a conventional polarizing beam splitter (PBS), unpolarized light is split into orthogonal polarizations with equal intensity. Therefore, for two output splitting, a half-wave plate (HWP) and quarter-wave plate (QWP) are necessary to convert the beam into any arbitrary polarization (Fig. S1(a)). We showed in the previous section that only 50:50 power splitting ratio is possible for two outputs in the ideal case.

For unpolarized light conversion and arbitrary power splitting between three or more outputs, we identify a scheme that involves an additional series of Mach-Zehnder interferometers (MZI) and phase shifters (PS), see Figs. S1(b,c). We note that for a general $N\times N$ system that can perform arbitrary power distribution at the output, $N(N-1)/2$ interferometer unit cells are required[56,57]. Thus, for an increasing number of outputs, the complexity of the interferometer layout rapidly grows. Furthermore, there appears a highly challenging requirement of phase stability between multiple optical components. As a result, ensuring the correct power splitting ratios would be unfeasible for consumer end-user applications based on bulk optics. In contrast, our metasurface is able to dramatically decrease the system footprint while avoiding the issue of phase stability since all the interference stages happen completely in a single nanostructured layer.

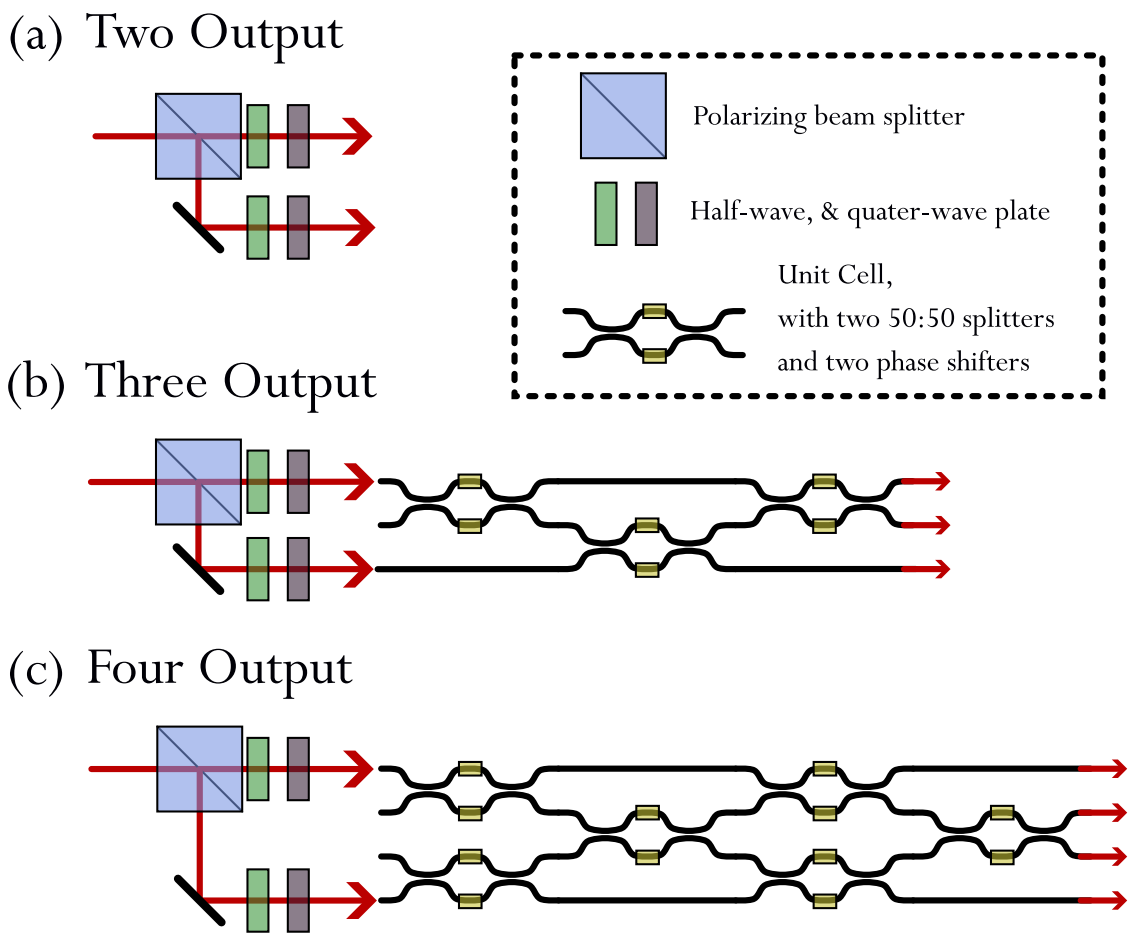

Figure S1. Theoretical designs for different multi-output schemes with conventional optical components. To achieve arbitrary power splitting and polarization conversion of unpolarized light, a series of polarizing beam splitters, half-wave plates, quarter-wave plates, Mach-Zehnder interferometers, and phase shifters are required.

S3. INVERSE DESIGN METHOD

Here we derive the exact expressions that were used as part of the optimization. The FOM used in the optimization is

$$FOM = \prod_n \left[|\langle \psi | \mathbf{J}_n|^2 - |\langle \psi_\perp | \mathbf{J}_n|^2 \right], \tag{S12}$$

where $|\psi\rangle$ is the desired output polarization state for all diffraction orders, and $|\psi_\perp\rangle$ is an undesired orthogonal state ($\langle\psi|\psi_\perp\rangle = 0$). The FOM is a series product over different diffraction terms, which acts similarly to a self-modulating weighted sum. Each element of $\mathbf{J}_n$ for the n^{th} diffraction order

is a scattering coefficient

$$\mathbf{J} = \begin{pmatrix} a_{xx} & a_{xy} \\ a_{yx} & a_{yy} \end{pmatrix} \tag{S13}$$

One can show that the permittivity derivative is[41]

$$\frac{\partial a_{xx}}{\partial \varepsilon} = i\omega \mathbf{E}_x^{\text{for}} \mathbf{E}_x^{\text{adj}}. \tag{S14}$$

We let $\langle \psi | = \begin{bmatrix} A & B \end{bmatrix}$, then its orthogonal vector is $\langle \psi_\perp | = \begin{bmatrix} B^* & -A^* \end{bmatrix}$. The expression from Eq. (S12), for a given n, can be expanded to be

$$FOM = |Aa_{xx} + Ba_{yx}|^2 + |Aa_{xy} + Ba_{yy}|^2 - |B^* a_{xx} - A^* a_{yx})|^2 - |B^* a_{xy} - A^* a_{yy}|^2 \tag{S15}$$

We can then write the derivative of the figure of merit with respect to each element of the Jones matrix

$$\frac{\partial FOM}{\partial a_{xx}} = A(Aa_{xx} + Ba_{yx})^* - B^*(B^* a_{xx} - A^* a_{yx})^* \tag{S16}$$

$$\frac{\partial FOM}{\partial a_{xy}} = A(Aa_{xy} + Ba_{yy})^* - B^*(B^* a_{xy} - A^* a_{yy})^* \tag{S17}$$

$$\frac{\partial FOM}{\partial a_{yx}} = B(Aa_{xx} + Ba_{yx})^* - A^*(B^* a_{xx} - A^* a_{yx})^* \tag{S18}$$

$$\frac{\partial FOM}{\partial a_{yx}} = B(Aa_{xy} + Ba_{yy})^* - A^*(B^* a_{xy} - A^* a_{yy})^* \tag{S19}$$

Then using the chain rule with the above expressions, we get

$$\frac{\partial FOM}{\partial \varepsilon} = \frac{\partial FOM}{\partial a_{xx}} \frac{\partial a_{xx}}{\partial \varepsilon} + \frac{\partial FOM}{\partial a_{xy}} \frac{\partial a_{xy}}{\partial \varepsilon} + \frac{\partial FOM}{\partial a_{yx}} \frac{\partial a_{yx}}{\partial \varepsilon} + \frac{\partial FOM}{\partial a_{yy}} \frac{\partial a_{yy}}{\partial \varepsilon} + c.c. \tag{S20}$$

Because the FOM is a real function, we do not have to evaluate the complex conjugate in reality, and may instead just calculate

$$\frac{\partial FOM}{\partial \varepsilon} = 2\,\mathrm{Re}\left\{ \frac{\partial FOM}{\partial a_{xx}} \frac{\partial a_{xx}}{\partial \varepsilon} + \frac{\partial FOM}{\partial a_{xy}} \frac{\partial a_{xy}}{\partial \varepsilon} + \frac{\partial FOM}{\partial a_{yx}} \frac{\partial a_{yx}}{\partial \varepsilon} + \frac{\partial FOM}{\partial a_{yy}} \frac{\partial a_{yy}}{\partial \varepsilon} \right\} \tag{S21}$$

Then for the i^{th} iteration, a gradient ascent method is used for optimization

$$\varepsilon_{i+1}(\mathbf{x}) = \varepsilon_i(\mathbf{x}) + \frac{\partial FOM}{\partial \varepsilon} \Delta t \tag{S22}$$

where Δt is the step size. We plot the progression of the FOM during optimization for the metasurface design in the manuscript (Fig. S2).

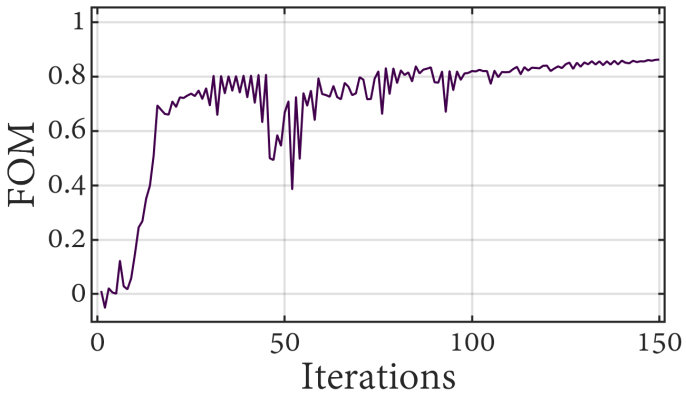

Figure S2. Convergence of the FOM for the metasurface diagonal polarizer shown in the main manuscript.

S4. METASURFACE JONES MATRIX ANALYSIS

The Jones matrix represents the complex scattering of incident light as it transmits through the metasurface. We use the RCWA solver RETICOLO[46] to calculate the transmitted complex amplitude for each element of the Jones matrix.

For the metasurface design presented in Fig. 2 of the main manuscript operating at $\lambda = 1550\,\mathrm{nm}$ wavelength and $\alpha = 45^\circ$ incidence angle, the Jones matrices in the $H - V$ basis at the zeroth and first diffraction orders, respectively, are

$$J_0^{HV} = \begin{pmatrix} 0.4042 + 0.0000i & 0.5348 + 0.1159i \\ -0.4302 + 0.0689i & -0.4797 - 0.2105i \end{pmatrix} \tag{S23}$$

$$J_1^{HV} = \begin{pmatrix} 0.4793 + 0.0000i & -0.3067 - 0.2136i \\ -0.4885 - 0.0343i & 0.4494 + 0.2266i \end{pmatrix} \tag{S24}$$

The phases have been normalized such that all elements are relative to the first element of the matrix. Then, singular value decomposition (SVD) of these matrices is used to understand the input and output polarization states with maximum transmission (Fig. S3). The ratio of the square of singular values is equivalent to the extinction ratio. We see that for both diffraction orders, the maximum transmitted output polarization state is the D state, with extinction ratios on the order of 100. On the other hand, the maximum transmitted input polarization state is some elliptical polarization. It is worth noting that this pair of elliptical states differs between the diffraction orders, but are almost orthogonal to each other. We note that for two outputs, if one polarization is maximally transmitted for one output, then its orthogonal polarization must be maximally transmitted into the

other output in the ideal case (Section S1.2). The challenge, which our metasurface addresses, is converting both of these outputs into the same polarization state.

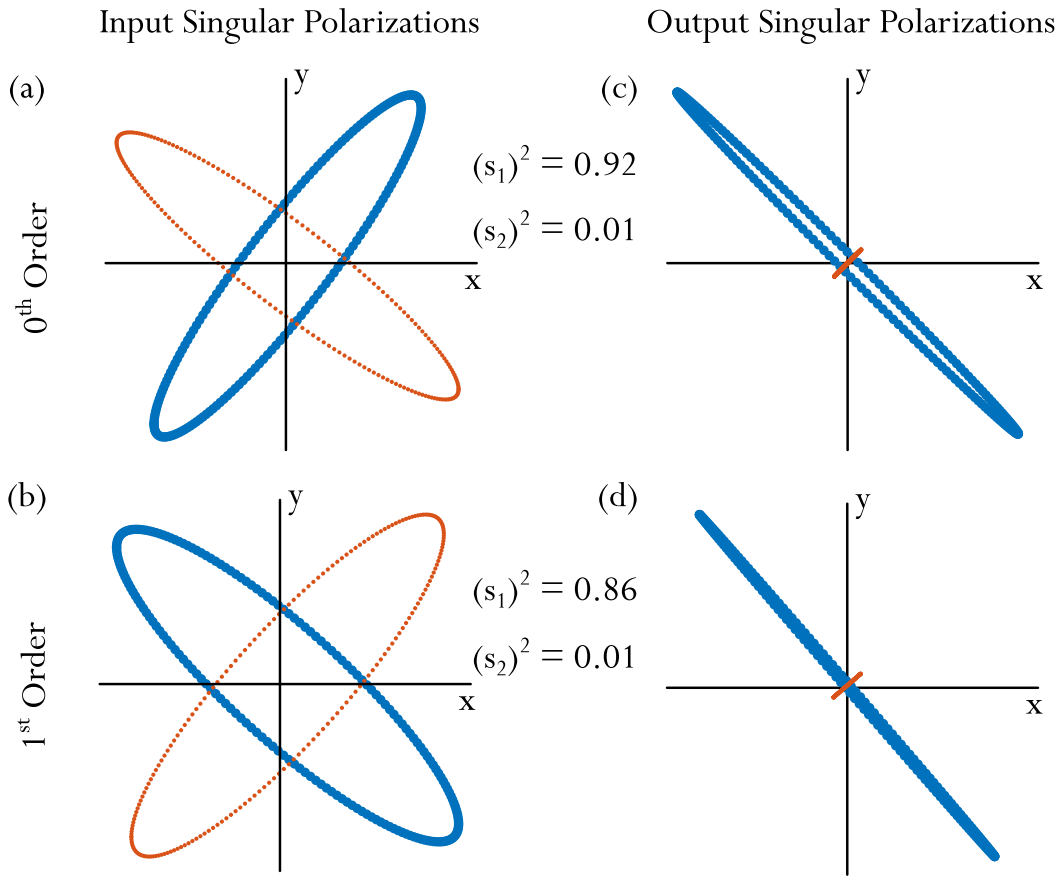

Figure S3. Orthogonal singular polarization states for the two diffraction orders that produce the maximum and minimum singular values, s_1 (blue lines) and s_2 (red lines) respectively. (a,b) Input singular polarizations for 0^{th} and 1^{st} order respectively. (c,d) Output singular polarizations for 0^{th} and 1^{st} respectively, with amplitudes normalized to the singular value.

In this form of the Jones matrices, it is not immediately obvious what transformation the metasurface is applying on the incident light. To make this more clear, we can perform a change of basis to another representation of the Jones matrix in the form of

$$J^{DA/HV} = \begin{pmatrix} t_{DH} & t_{DV} \\ t_{AH} & t_{AV} \end{pmatrix}, \tag{S25}$$

where D and A are orthogonal diagonal and anti-diagonal vectors. This representation directly relates to the polarization capability of the metasurface and reflects how our measurements were

performed. Then for zeroth and first order respectively,

$$\mathcal{J}_0^{DA/HV} = \begin{pmatrix} 0.5920 + 0.0000i & 0.6959 + 0.2890i \\ 0.0223 - 0.0470i & -0.0443 + 0.0635i \end{pmatrix} \tag{S26}$$

$$\mathcal{J}_1^{DA/HV} = \begin{pmatrix} 0.6848 - 0.0000i & -0.5454 - 0.2921i \\ 0.0074 + 0.0240i & -0.1012 - 0.0056i \end{pmatrix}. \tag{S27}$$

Let us round the elements in the above expressions to 1 decimal place for ease of clarity in the following discussion:

$$\mathcal{J}_0^{DA/HV} \simeq \begin{pmatrix} 0.6 & 0.7 + 0.3i \\ 0 & 0.1i \end{pmatrix} \tag{S28}$$

$$\mathcal{J}_1^{DA/HV} \simeq \begin{pmatrix} 0.7 & -0.5 - 0.3i \\ 0 & -0.1 \end{pmatrix}. \tag{S29}$$

As an example, we can interpret the element t_{DH} as the complex amplitude of the scattering of H polarized input into D polarized output. From $\mathcal{J}_0^{DA/HV}$, we see that scattering of incoming light into D polarization dominates scattering into A polarization. This is also the case for the first diffraction order $\mathcal{J}_1^{DA/HV}$. It is also interesting to observe that there is a similar magnitude of t_{DH} and t_{DV} elements for both diffraction channels. Therefore, we can deduce there is significant conversion of both H and V states into the D state in order to overcome the 50% limit. From these matrices of both orders, we see that there is almost no transmission into the A state, and thus the output polarization would have a high extinction ratio.

S5. MULTIPOLAR DECOMPOSITION OF FIELDS IN NANORESONATOR

One method to gain insight into the physics that underpins the action of a resonator is to decompose the fields generated into higher-order multipoles. We follow the equations in Table II of reference[48] to calculate the values of the electric dipole (ED), magnetic dipole (MD), electric quadrupole (EQ), and magnetic quadrupole (MQ) moments under oblique incidence ($\alpha = 45°$) that mimics the operation of the metasurface. The choice of origin is set to be at the center of the unit cell (coordinate (X,Y) = $(450\,\mathrm{nm}, 450\,\mathrm{nm})$ in Fig.2(c) of the main manuscript). Once the moments have been determined, one may calculate their respective scattering contributions. From Fig. S4, we observe that the fields are strongly associated with ED moments for $|H\rangle$ and $|V\rangle$ input

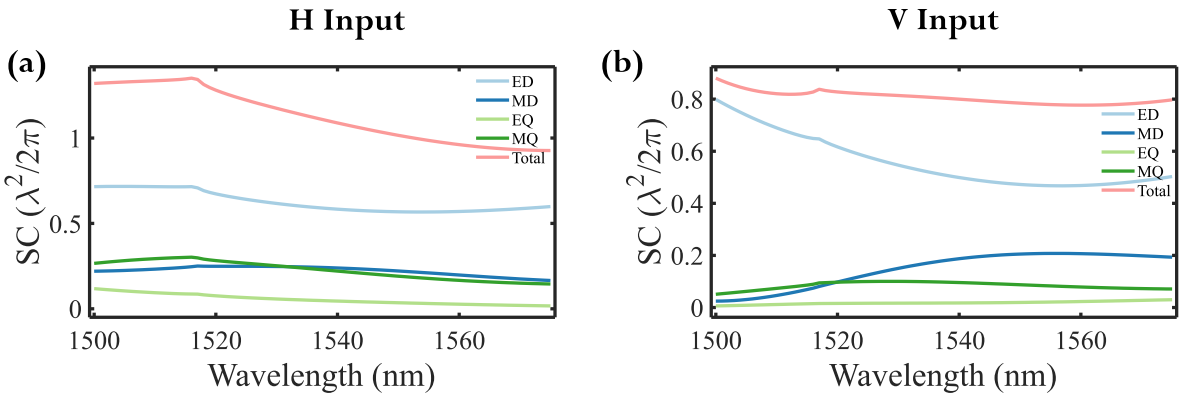

Figure S4. Mode decomposition for (a) H-polarized input and (b) V-polarized input into the electric dipole (ED), magnetic dipole (MD), electric quadrupole (EQ), and magnetic quadrupole (MQ) moments of the metasurface design in Fig. 2 of the main manuscript.

states, with quadrupole moments being suppressed. The feature observed at around 1516 nm is due to the disappearance of the first-order reflective diffraction order in the y-direction into the substrate as the wavelength increases. We note that there is no first order reflection into the air in the y-direction for the entire wavelength range of interest. Moreover, there is a lack of strong resonant features across the entire wavelength range. This is the reason the metasurface response has a flat response as needed for the application.

We then perform these same decompositions for maximum and minimum transmitted polarization states as inputs from Fig. S3 for the 0^{th} and 1^{st} diffraction order (Fig. S5). For the 0^{th} order (Fig. S5(a)) and the maximally transmitted polarization, the total scattering is relatively constant over the entire wavelength range with the strongest scattering being due to the ED moments. We further break down the component contributions to ED and MD moments (2nd and 3rd columns). The presence of large z components in the dipole moments is not unexpected since the beams are travelling at oblique incidences. For the case of the 1^{st} diffraction order, the maximally transmitted polarization state is almost orthogonal to that of the 0^{th} order. Therefore, we expect to see the calculated scattering cross-sections for the 0^{th} order almost be reversed for the 1^{st} order, and we indeed observe this to be the case (Fig. S5(b)). This dual response from orthogonal polarizations (Figs. S4,S5) is what enables the metasurface to have a uniform response from an unpolarized source and to break the 50% conversion limit.

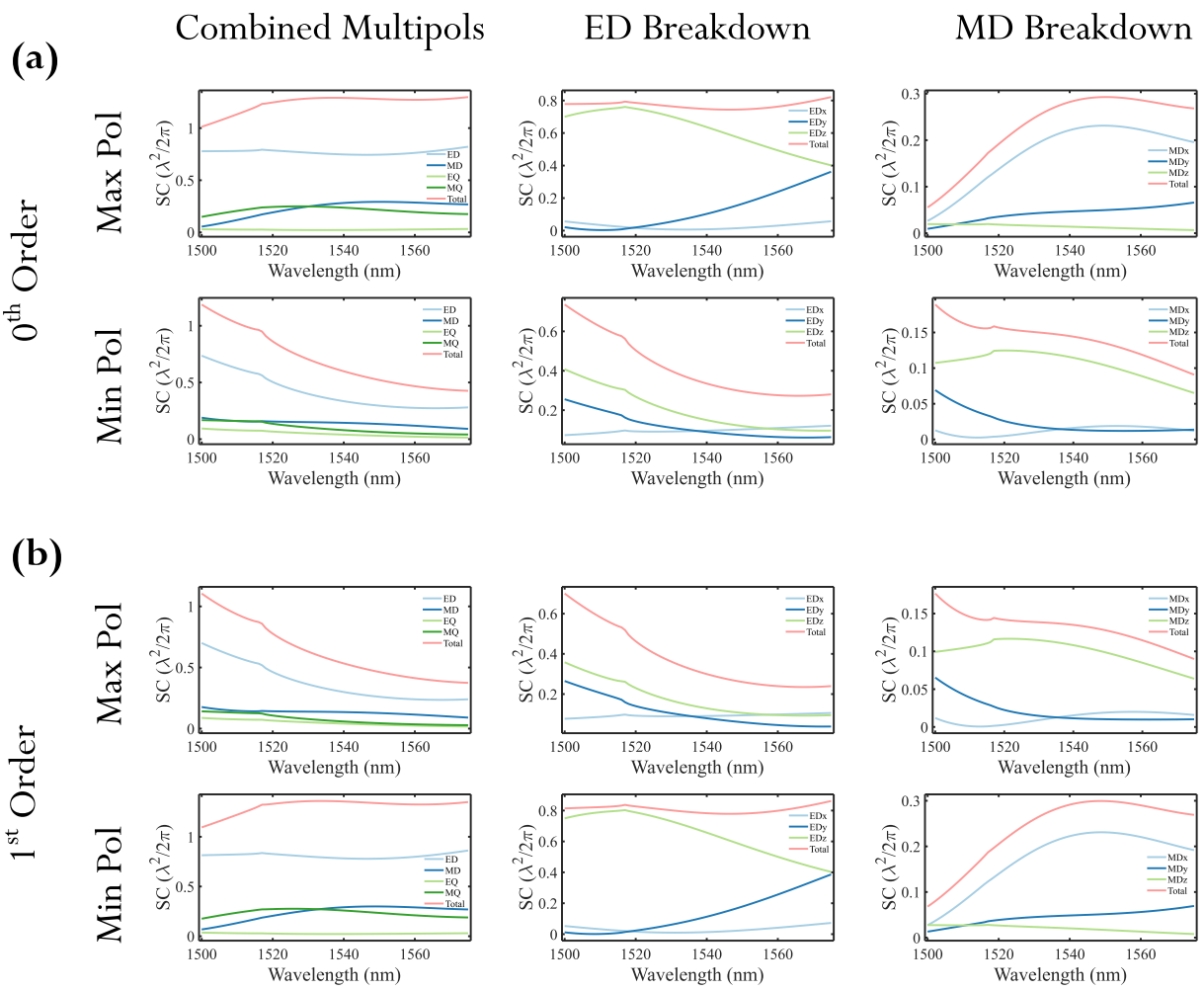

Figure S5. Mode decomposition for maximally and minimally transmitted polarizations (from Fig. S3) of the (a) 0^{th} order and (b) 1^{st} order respectively. The ED and MD moments are further decomposed into their respective orthogonal components.

S6. COMPARISON OF OUR WORK TO OTHER METASURFACE AND COMMERCIALLY AVAILABLE POLARIZERS

Metasurface polarizers have been widely researched in the community. Theoretically, guided-mode resonances may produce an infinite extinction ratio[49], while in experiments, there have been demonstrations of metasurfaces that produce extinction ratios greater than 10,000[50]. Commercial polarizers have extinction ratios that range between 10 and 100,000 depending on the fabrication complexity and associated cost[51]. While these examples all have much larger extinction ratios than what we have demonstrated, we emphasize that the key result of our work is the proposal and experimental demonstration of the total transmission efficiency of converting unpolarized light

into a target output polarization that is greater than the 50% fundamental limit of single-output polarizers. All the aforementioned examples are indeed limited to the 50%. In future work, the maturing technology for multi-layer or volumetric metamaterials[52,55] may provide a path to even larger extinction ratios beyond what is possible with single-layer metasurfaces.

S7. INCIDENT ANGLE DEPENDENCY

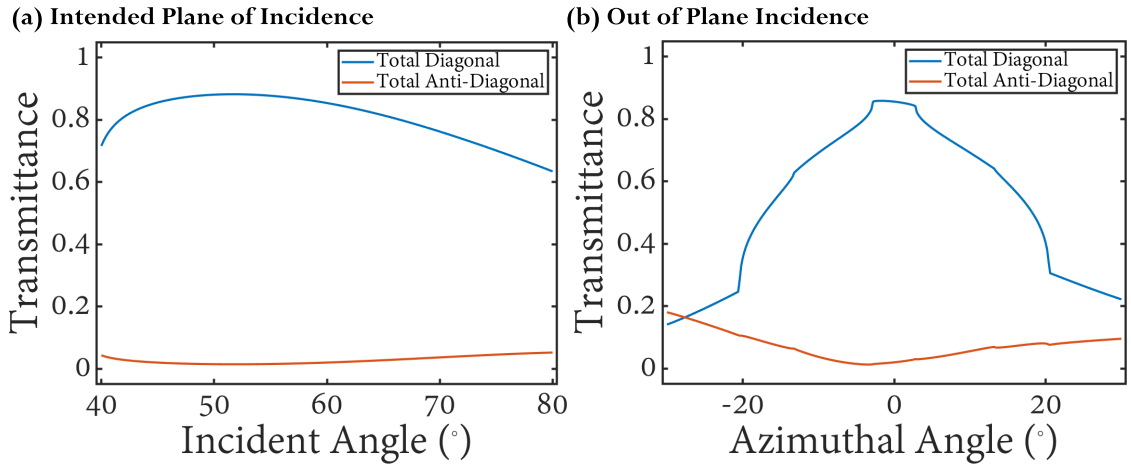

Figure S6. Combined polarization efficiency as a function of incident angle for (anti)-diagonal polarization along (a) the intended plane of incidence, and (b) out of plane incidence for a range of azimuthal angles at fixed $\alpha = 45°$.

The metasurface presented in Fig. 2 of the main manuscript was designed with an intended $45°$ incident angle along one axis. In Fig. S6(a), we can see that indeed, this is the case. Furthermore, this near-optimal performance has a large angle range, extending from $\sim 42°$ to over $60°$, where the total polarization transmittance to the desired diagonal state exceeds 0.8. In fact, for the entire range $40°$ to $80°$, this transmittance exceeds 0.6, which is beyond the fundamental polarization conversion limit of 0.5 for unpolarized light. We note that within this range, the metasurface is in the regime where only 2 diffraction orders are permitted. Due to technical limitations of our experimental setup, large incident angles onto the metasurface were not measured.

We also simulate the metasurface under the target incident angle ($\alpha = 45°$) for a range of azimuthal angles (Fig. S6(b)). It is apparent that the metasurface does have similar performance characteristics at small azimuthal angles. It is only beyond $\pm 5°$ azimuthal angle that significantly lower transmission efficiencies become apparent. This is not unexpected, as the asymmetrical

nature of the metasurface unit cell means that the electromagnetic scattering is sensitive to the plane of incidence. Such performance is suitable for optical systems with numerical aperture smaller than approximately 0.1, which is the case for our experiments.

S8. SIMULATING UNPOLARIZED LIGHT WITH POLARIZED SOURCES

Unpolarized light can be formed by an incoherent combination of orthogonal states. These orthogonal input polarization states for the experiment are vertical $|V\rangle$ and horizontal $|H\rangle$, which are prepared and projected through the metasurface. For each *input* polarization state, the corresponding *output* polarization states were analyzed at each diffraction order by measuring the powers in the diagonal $|D\rangle$ and anti-diagonal $|A\rangle$ polarization components. By combining results, we may effectively determine the response of the metasurface to unpolarized light. For example, P_{D,V_0} is defined as measuring the power output projected to $|D\rangle$ with input $|V\rangle$ for the zeroth order. We then infer the power for $|D\rangle$ polarization in the zeroth order for an unpolarized input by averaging the measurements as $P_{D_0} = \frac{1}{2}(P_{D,V_0} + P_{D,H_0})$, and this is similarly done for the first order P_{D_1}.

S9. CALIBRATION OF MEASUREMENTS

We perform calibration measurements to set a baseline for the experimental setup. We illuminate the detector without any metasurface in the beam path. The only optical components in the beam path are the lenses, polarizers and wave-plates needed for characterization. Initial polarization is prepared with a prism aligned to the $|H\rangle$ state and analyzed with another prism in the $|D\rangle$ state. We perform this measurement for every combination of $|H\rangle$ and $|V\rangle$ inputs, and $|D\rangle$ and $|A\rangle$ outputs for a total of four independent measurements. For example, $P_{D,V}$ is the power measured when the input of $|V\rangle$ is analyzed in $|D\rangle$. We confirm that $P_{D,V} = P_{D,H} = P_{A,V} = P_{A,H} = \frac{1}{2}P_{V,V} = \frac{1}{2}P_{H,H}$ up to a negligible measurement error. This also calibrates the polarizers' orientation relative to each other. Our tunable illumination source is swept from $1500\,\mathrm{nm}$ to $1575\,\mathrm{nm}$ which covers the spectral range of interest.

In our experiment, we simultaneously measure the power of each of the two output beams of the metasurface. Thus, we have two power meters that are in operation at the same time. To account for different detector sensitivities, identical calibration measurements, outlined above, were performed. When we then measure the metasurface performance, the variation in detector

sensitivity is taken into account through the calibration data.

S10. TWO-OUTPUT CIRCULAR POLARIZER: DESIGN AND EXPERIMENTS

We also can produce a circular polarizer design in much the same way as the diagonal polarizer presented in the main paper. The angle of incidence is once again $45°$. The converged pattern is close to a widened horseshoe (Fig. S7(a)). Conversion efficiencies into the circular polarization state for the two outputs have similar magnitudes across the intended spectral range. We predict that the total conversion efficiency of unpolarized light into circular polarization exceeds 80% at $1550\,\mathrm{nm}$ (Fig. S7(b)), with a combined maximum extinction ratio of $\sim$40 at $1530\,\mathrm{nm}$ (Fig. S7(c)). Similar to Fig. S6, this circular polarizer has a transmittance that exceeds 60% for the entire range $40°$ to $80°$, which is beyond the fundamental polarization conversion limit of 50% for unpolarized light.

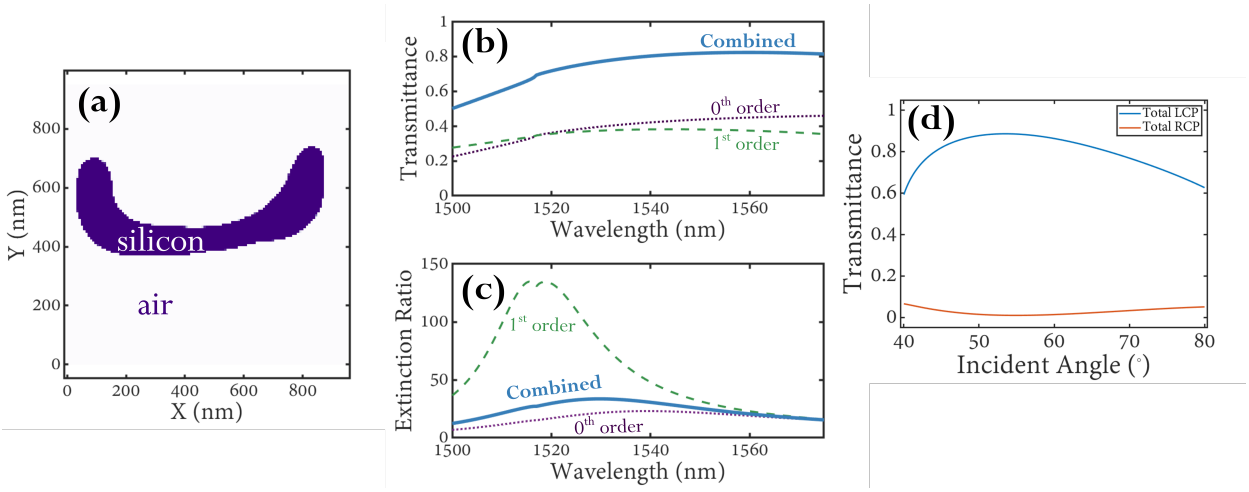

Figure S7. (a) Geometry of the metasurface pattern optimized for the target left circular polarization at two diffraction orders. (b) Conversion efficiency of outputs to the desired circular polarization state from an unpolarized source, and (c) their respective extinction ratios. (d) Incident angle dependency of the metasurface transmission to the target (LCP) and undesired (RCP) polarization components.

We fabricate the circular polarizer and perform measurements in a similar manner outlined in the main manuscript (Fig. S8(a)). The only difference is that an additional quarter-wave plate is placed after the metasurface and before the polarizer (Fig. S8(b)). This converts circular polarization into diagonal polarization. To quantify the metasurface's performance under unpolarized

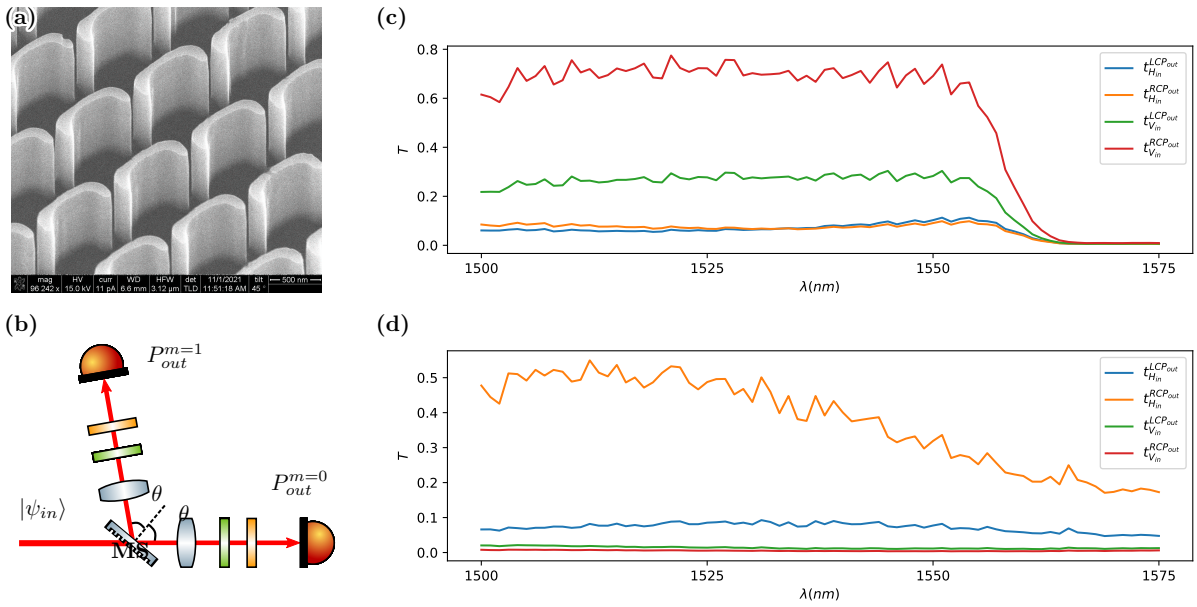

Figure S8. (a) Fabricated metasurface design from Fig. S7(a). (b) Experimental setup for the characterization of the metasurface. (c,d) Experimentally measured total output transmissions $t_{Pol_{in}}^{Pol_{out}}$ for a given polarization input and output, denoted by the sub- and super-scripts, at the 0th and 1st transmission orders, respectively.

illumination, we prepare vertical (V) and horizontal (H) polarization from the laser source. Then we take measurements for each combination of input state (V and H) and output orthogonal state (LCP and RCP) for the two output beams (Fig. S8(c,d). This information allows us to reconstruct the combined metasurface performance in terms of total conversion efficiency of unpolarized light and extinction ratio (Fig. S9(a,b)). We observe experimentally that the metasurface does surpass the 50% conversion efficiency limit in the wavelength range $1500\,\mathrm{nm}$ to $1550\,\mathrm{nm}$. We believe that the sudden drop in transmittance for the longer wavelengths can be attributed to the changing output beam angle as the wavelengths are swept. This causes the position of the beam to wander across the detector surface. This issue was mitigated for the measurements presented in the main paper by placing a lens before the detector.

S11. PERFORMANCE TOLERANCE FOR DILATED AND ERODED STRUCTURES

Although the manufactured dimensions of the metasurface are very close to the design dimensions, slight deviations can cause deterioration of the performance in polarization conversion

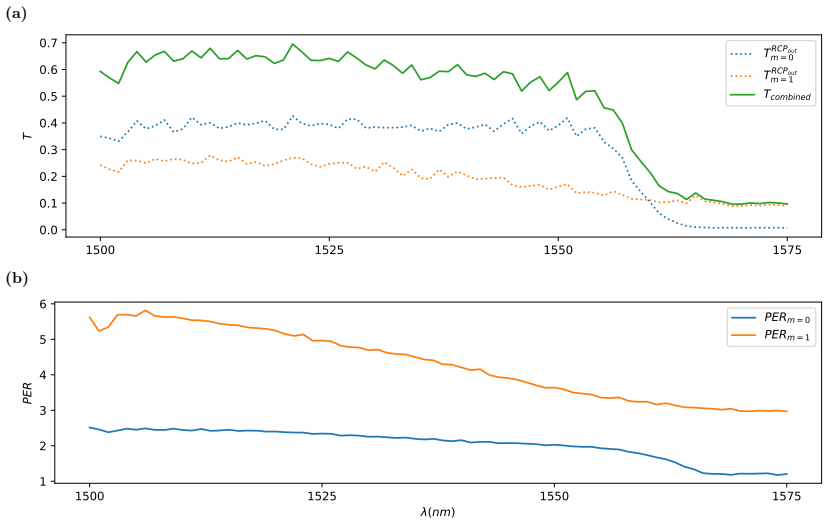

Figure S9. (a) Total transmitted conversion efficiency of unpolarized input into the target right circular polarization state measured experimentally. (b) The corresponding polarization extinction ratios for each of the outputs.

efficiency. We try to alleviate this issue by increasing the robustness of the design to fabrication processes during the optimization. This is achieved by applying a constant Gaussian 2D blur with a width of 50 nm to our pattern throughout the optimization, and thus smoothing out small features. We provide simulations of dilated and eroded structures, which show that our design has a high robustness on manufacturing deviations. Further optimization of the etching process can ensure greater fidelity to the specified design, by decreasing tapering of the metasurface side-walls.

We provide the simulated performance of slightly eroded and dilated structures to gauge the tolerance of the metasurface to fabrication deviations (Fig. S10). The first row shows the performance for the optimized design, and is identical to the graphs in Fig. 2(f,g) of the main manuscript. The dilated structure (Fig. S10(b)) has much lower transmittance than required at shorter wavelengths, but still achieving greater than 50% conversion efficiency for longer wavelengths. For the eroded structure (Fig. S10), the transmittance is lower than in the optimized design, but is still greater than the 50% limit across the entire bandwidth. However, we note that the extinction ratio for both cases suffers in performance. Future work will aim to preserve large extinction ratios for even with fabrication imperfections.

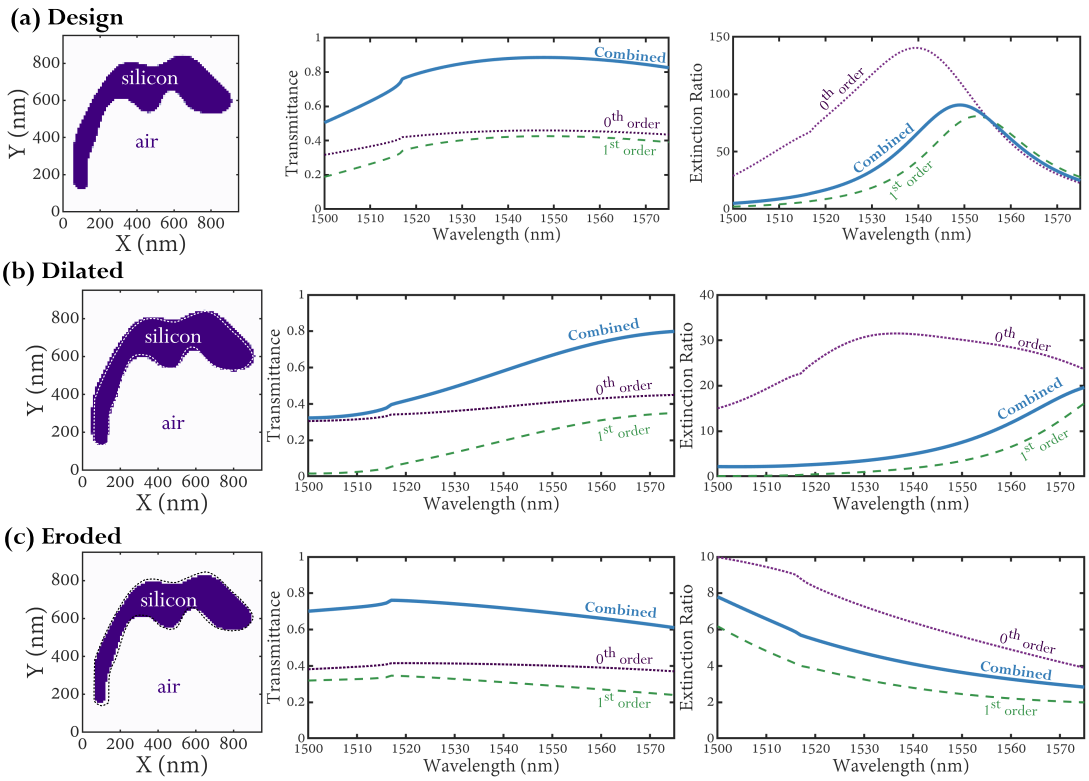

Figure S10. Simulated transmittances and extinction ratios for the (a) optimized, (b) dilated, and (c) eroded designs. The dashed lines over the patterns show the outline of the target design.

S12. METASURFACE DESIGN WITH $N = 4$ OUTPUTS

In addition to the 3-output design presented in the main paper, we optimize and show a 4-output design here. The incoming beam is at an incident angle of $45°$ in both the polar and azimuthal angles. The beam is then split in four different directions by the metasurface (Fig. S11(a)). The optimized pattern is shown in Fig. S11(b). The desired output state is H polarization. Simulations predict that the total conversion efficiency can surpass 80% over the wavelengths of $1530\,\mathrm{nm}$ to $1580\,\mathrm{nm}$ (Fig. S11(c)). Further, the combined extinction ratio of H to V polarizations is a maximum of 60 at the operating wavelength of $1550\,\mathrm{nm}$.

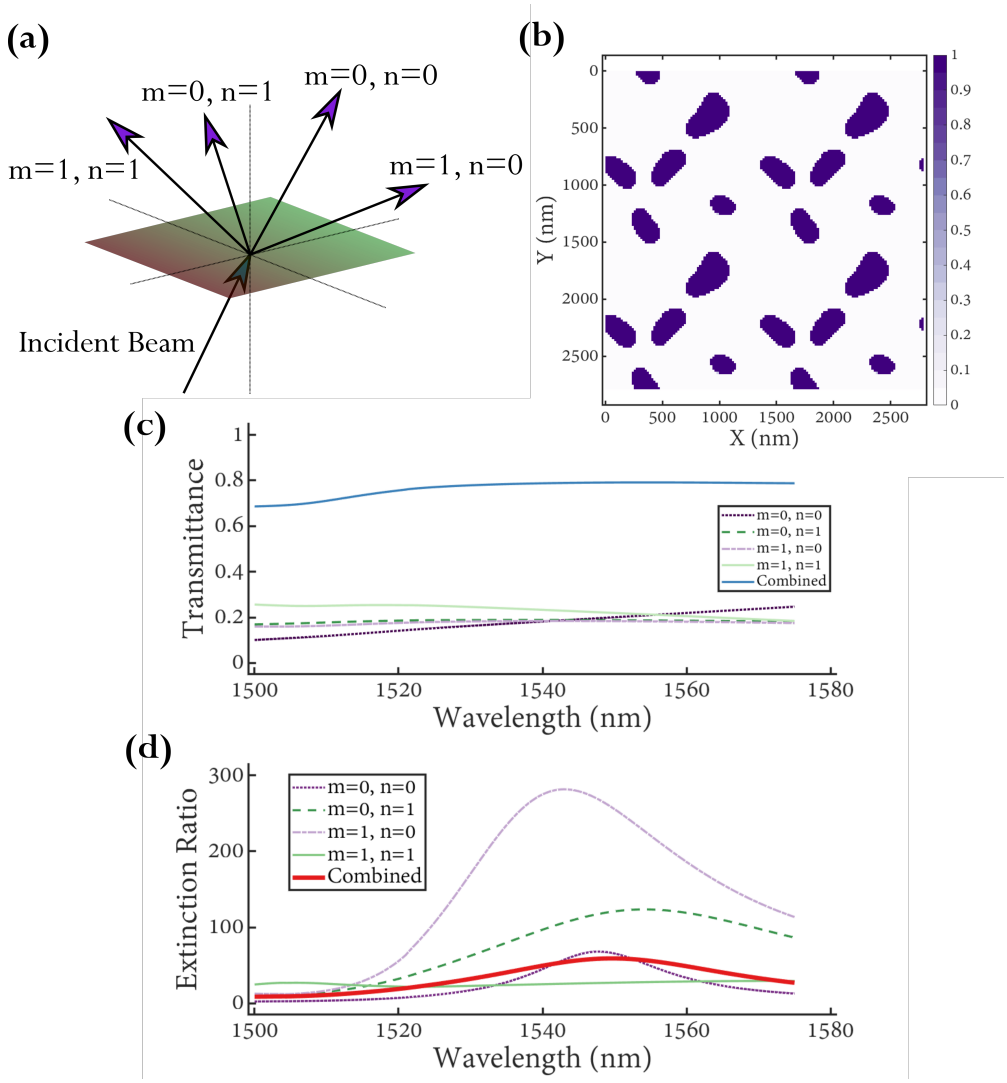

Figure S11. Design with four polarized outputs.(a) Diagram showing the four diffracted orders. (b) Final pattern for the metasurface. A 2-by-2 unit cell grid is shown. (c) Simulated transmittance of the metasurface of each diffraction order into the desired horizontal polarization state. (d) Extinction ratio of horizontal to vertical polarization state. The band between wavelengths 1540 nm to 1560 nm have optimal combined extinction ratio.